

Supplementary Information

Rapid Atmospheric Carbon Dioxide Fixation by Nickel(II) Complexes: Meridionally Coordinated Diazepane-based 3N Ligands Facilitate Fixation

Tamilarasan Ajaykamal,^a Mitu Sharma,^b Nasreen S. Islam^b and Mallayan Palaniandavar^{a*}

^aSchool of Chemistry, Bharathidasan University, Tiruchirappalli 620024, Tamilnadu, India

^bDepartment of Chemical Sciences, Tezpur University, Tezpur, Assam, India

Computed Structures of 1 and 2. We have performed computational analysis by using Density Functional Theory (DFT). And the optimized geometry of complexes **1** and **2** are shown in **Fig S1**. The computed structural parameters of the complexes are provided in Table S2.

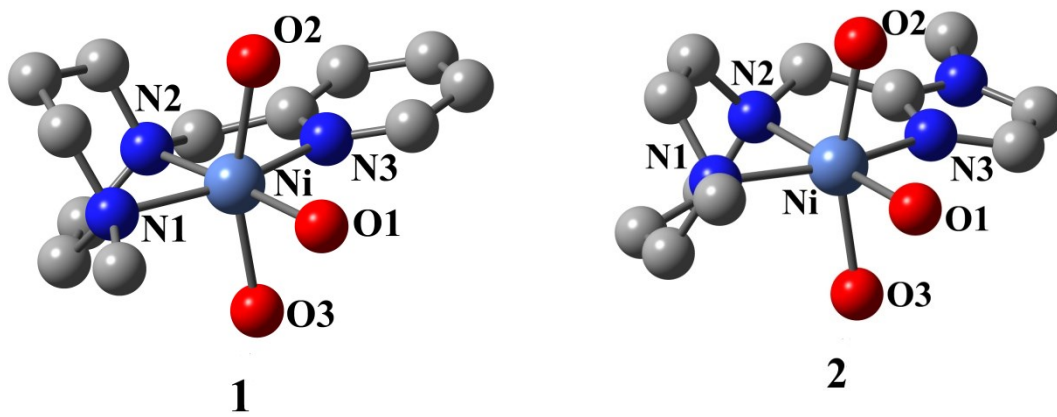


Fig. S1. The computed structures of cations of a) $[\text{Ni}(\text{L1})(\text{H}_2\text{O})_2](\text{ClO}_4)_2$ **1** and $[\text{Ni}(\text{L2})(\text{H}_2\text{O})_2](\text{ClO}_4)_2 \cdot 2\text{H}_2\text{O}$ **2**

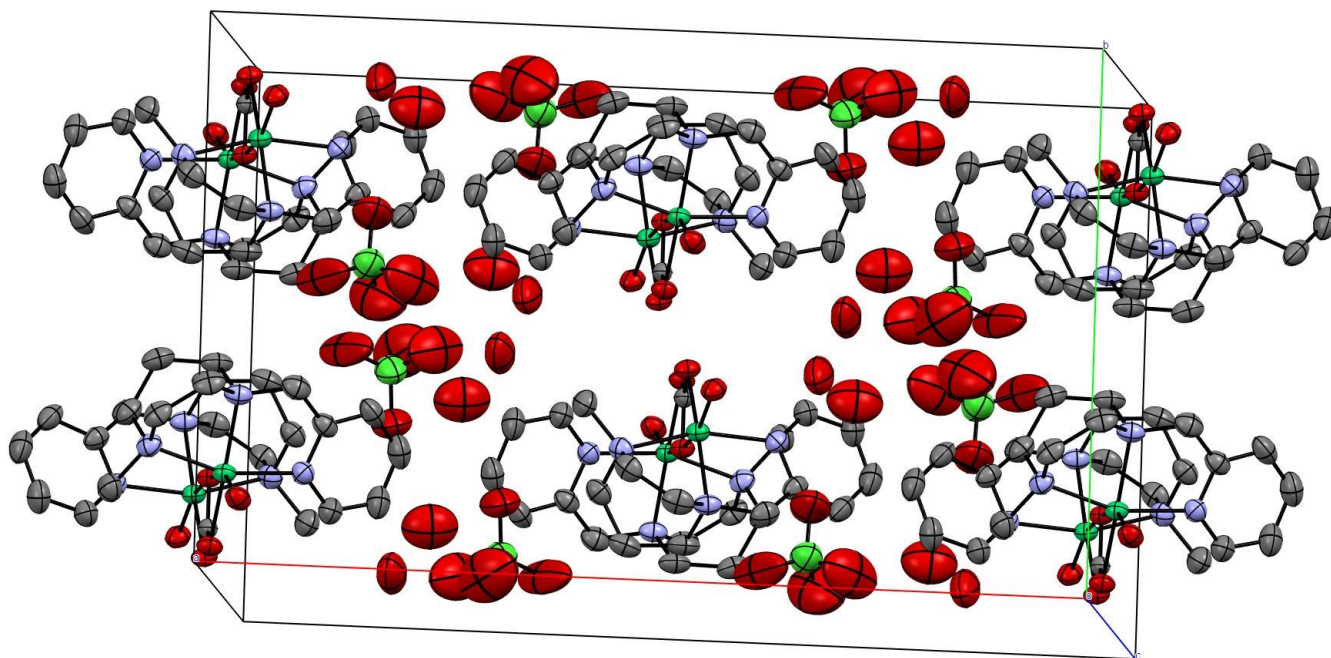


Fig. S2. The packing diagram of $[\text{Ni}_2(\text{L1})_2(\mu\text{-CO}_3)(\text{H}_2\text{O})_2](\text{ClO}_4)_2 \cdot 4\text{H}_2\text{O}$ **3**

Table S1. Structure refinement details for $[\text{Ni}_2(\text{L1})_2(\mu\text{-CO}_3)(\text{H}_2\text{O})_2](\text{ClO}_4)_2 \cdot 4\text{H}_2\text{O}$ **3**

3	
Sum formula	$\text{C}_{25}\text{H}_{42}\text{Cl}_2\text{N}_6\text{Ni}_2\text{O}_{17}$
Formula weight	886.96
Temperature (K)	296(2)
Wavelength (Å)	0.71073
Crystal system	monoclinic
Space group	C2/c
a(Å)	22.909(10)
b(Å)	14.148(6)
c(Å)	12.037(5)
α (°)	90
β (°)	101.433(6)
γ (°)	90
Volume (Å ³)	3824(3)
Z	4
D_c (g.cm ⁻³)	1.541
Reflections collected	25799
Goodness-of-fit on F ²	1.022
Final R indices [$I > 2\sigma(I)$]	0.0629, $wR_2 = 0.1710$
R indices (all data)	0.1049, $wR_2 = 0.2037$

Determination of magnetic moment of complex **1** and the intermediate derived from it

Evans' method was used of ^1H -NMR performed to determine the magnetic moment of complex **1** and the intermediate **1a** derived from it.^{S1-S2} A coaxial insert (with a sealed capillary) tube containing CD_3OD solvent (with 0.03% TMS) was inserted into the normal NMR tube containing the complex **1** (0.0053 M, with 0.03% TMS). We have calculated the chemical shift value of the TMS peak in the presence of the complex **1** in the outer NMR tube with respect to that of the TMS peak in the coaxial insert. The magnetic moment was calculated using the equation,

$$\begin{aligned}\mu_{\text{eff}} &= 0.0618 (\Delta\nu T / 2fM)^{1/2} \\ \mu_{\text{eff}} &= 0.0618 \times (32 \times 298 / 2 \times 400 \times 0.0053)^{1/2} \\ \mu_{\text{eff}} &= 2.93 \text{ BM}\end{aligned}$$

Where f = oscillator frequency (400 MHz) of the superconducting spectrometer, T = absolute temperature, M = molar concentration of the complex **1**, and ν = difference in frequency (Hz) between the two TMS signals (**Fig. S3**). The magnetic moment of complex **1** was calculated as 2.91 BM in CD_3OD at RT, suggesting the presence of 2 unpaired electrons in complex **1**. When Et_3N (0.0053 M, 50 μL) was added to this solution to generate a red coloured solution no shift was observed illustrating the formation of an intermediate species (low-spin) with no unpaired electron.

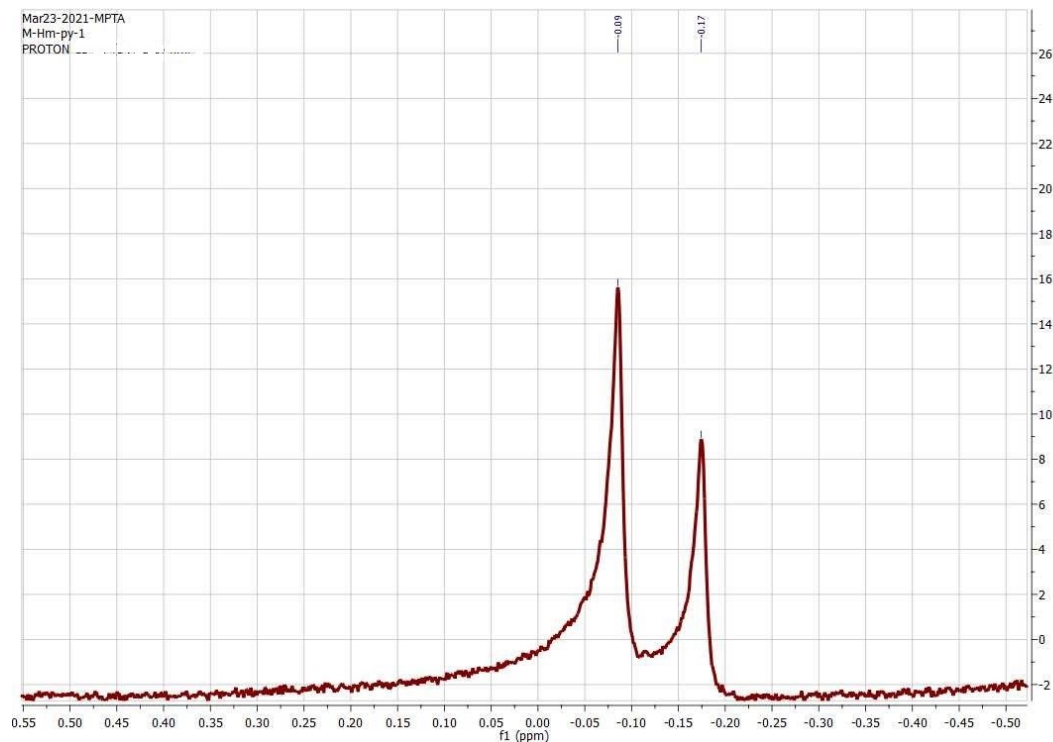


Fig. S3. Evan's method: ^1H NMR of spectra $[\text{Ni}(\text{L1})(\text{H}_2\text{O})_2](\text{ClO}_4)_2$ **1**

Table S2. Computed bond angles [°] of complexes **1**, **2** and the intermediates **1a** and **2a**

	1	2	1a	2a
N1–Ni–N2	77.9233	77.6300	83.15489	83.0770
N1–Ni–N3	160.9597	160.4098	168.9002	168.2117
N1–Ni–O1	102.1390	100.0281	100.2062	100.5885
N1–Ni–O2	96.9739	98.6302	-	-
N1–Ni–O3	95.5328	94.97454	-	-
N2–Ni–N3	83.1128	82.78310	86.2089	85.2117
N2–Ni–O1	176.4011	176.7345	176.4794	176.2916
N2–Ni–O2	100.9030	100.96143	-	-
N2–Ni–O3	94.2153	93.7329	-	-
N3–Ni–O1	96.8947	99.5575	90.3757	91.1363
N3–Ni–O2	84.8690	84.6499	-	-
N3–Ni–O3	87.4837	86.5886	-	-
O1–Ni–O2	82.6746	84.1666	-	-
O1–Ni–O3	82.1922	81.5814	-	-
O2–Ni–O3	162.0853	161.7781		-

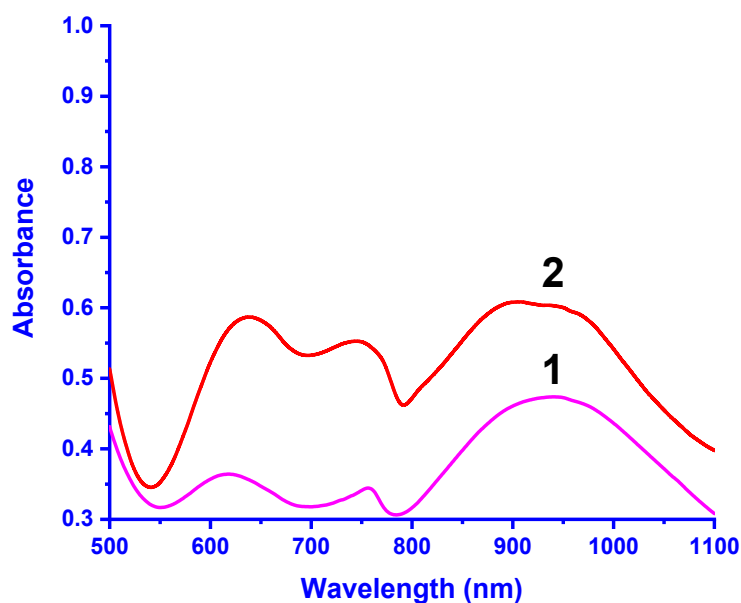


Fig. S4. Electronic absorption spectra of $[\text{Ni}(\text{L}1)(\text{H}_2\text{O})_3](\text{ClO}_4)_2$ **1** and $[\text{Ni}(\text{L}2)(\text{H}_2\text{O})_3](\text{ClO}_4)_2 \cdot 2\text{H}_2\text{O}$ **2** in methanol solution at 25 °C. Conc: **1**, 4.5×10^{-3} ; **2**, 3.3×10^{-3} M)

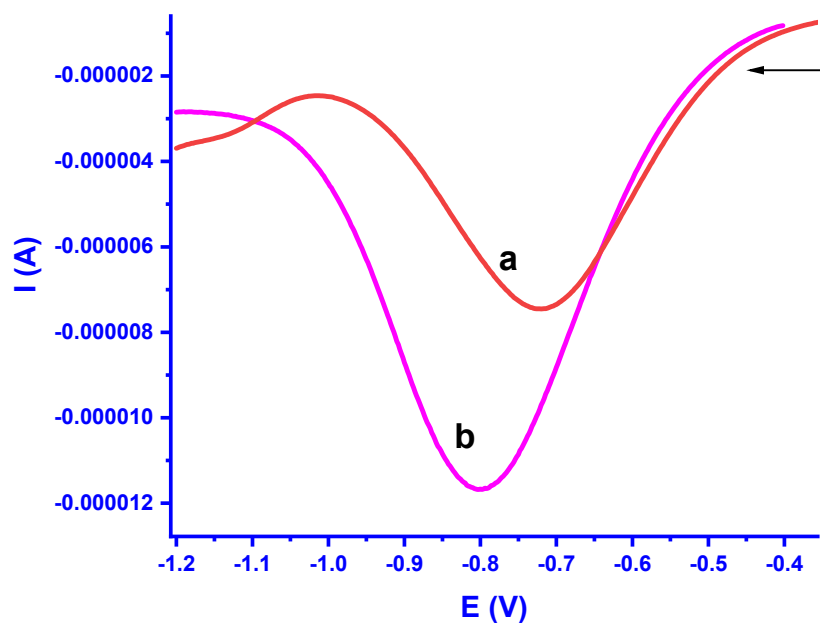


Fig. S5. Differential Pulse Voltammetry (DPV) of complexes **1** (1.9×10^{-3} M) and **3** (1.8×10^{-3} M) in methanol solution at 25 °C. Conditions: supporting electrolyte, 0.1 M TBAP; Scan rate, 50 mVs^{-1} ; reference electrode, Calomel; working electrode, Glassy carbon; Counter electrode, platinum plate

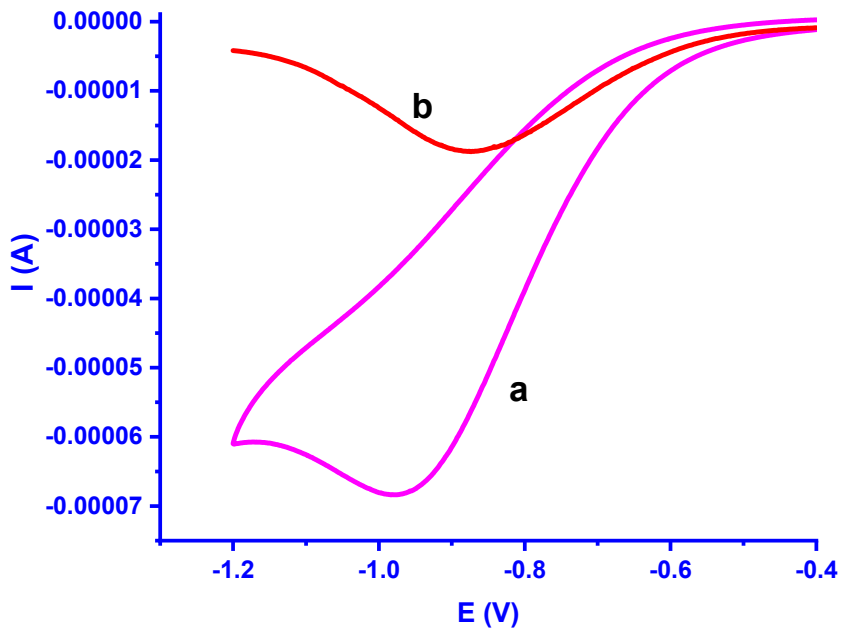


Fig. S6. Cyclic voltammogram (a) and DPV (b) of complex **2** (5.2×10^{-3}) in methanol solution at 25 °C. Conditions: supporting electrolyte, 0.1 M TBAP; Scan rate, 50 mVs⁻¹; reference electrode, Calomel; working electrode, Glassy carbon; Counter electrode, platinum plate.

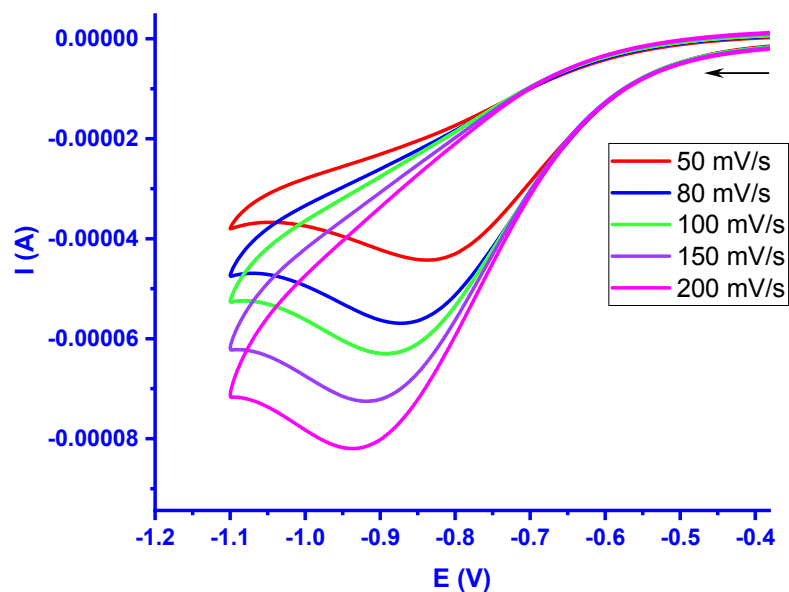


Fig. S7. Cyclic voltammograms of complex **1** (1.9×10^{-3} M) in methanol solution at 25 °C at different scan rates.

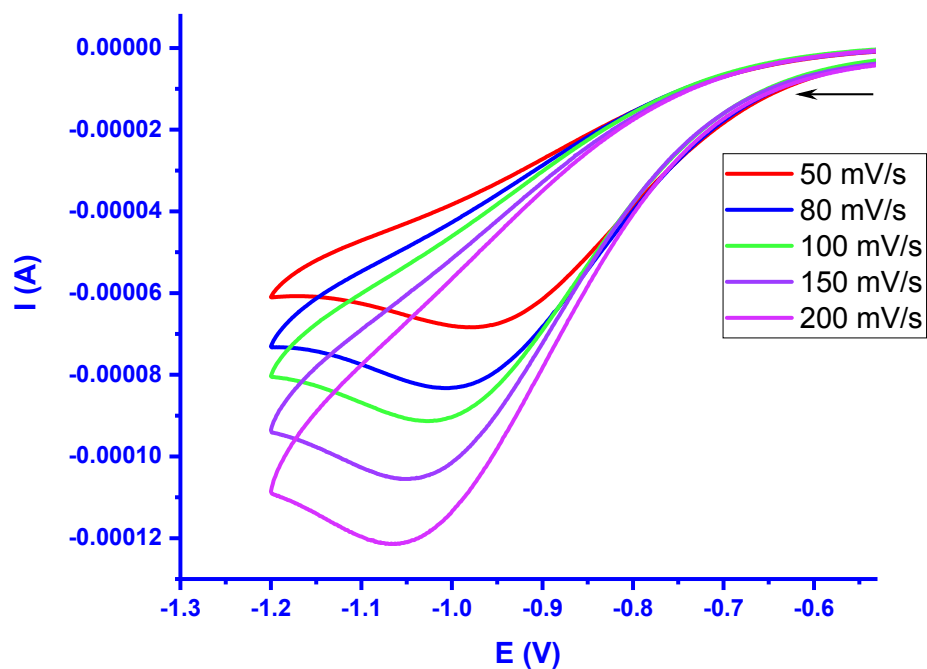


Fig. S8. Cyclic voltammograms of complex **2** (5.2×10^{-3}) in methanol solution at 25 °C at different scan rates.

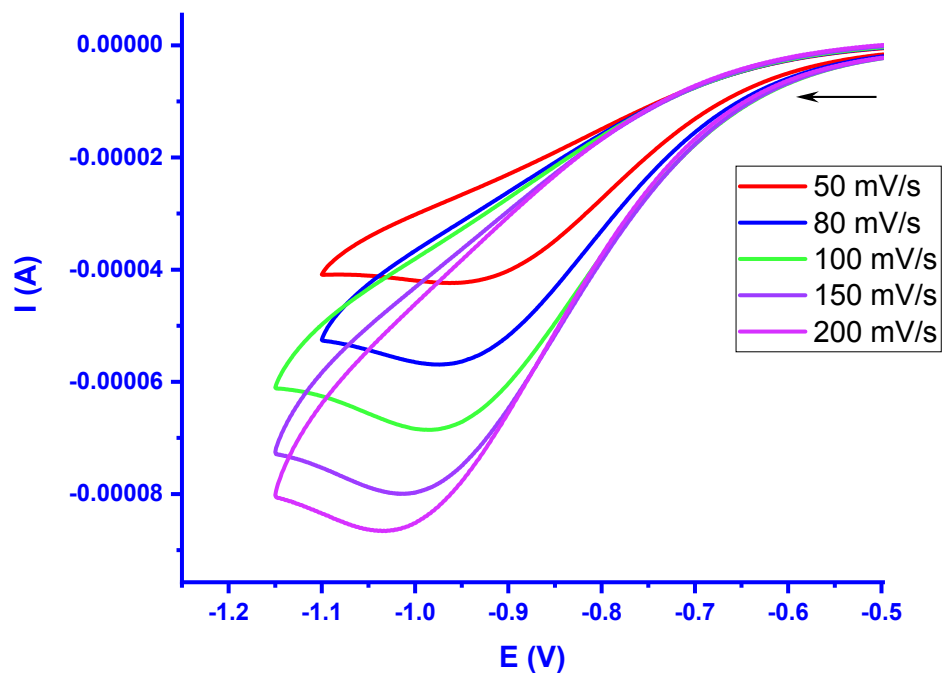


Fig. S9. Cyclic voltammograms of complex **3** (1.8×10^{-3} M) in methanol solution at 25 °C at different scan rates.

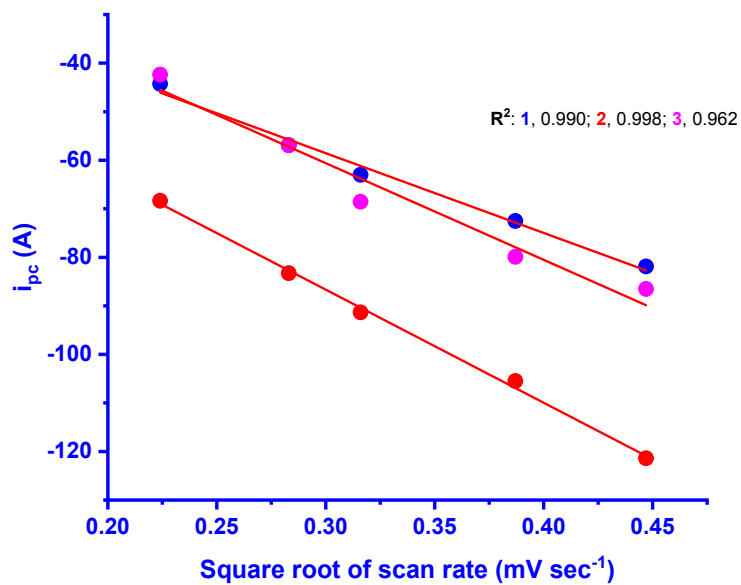


Fig. S10. Plots of i_{pc} (A) vs square root of scan rate (mV sec^{-1})

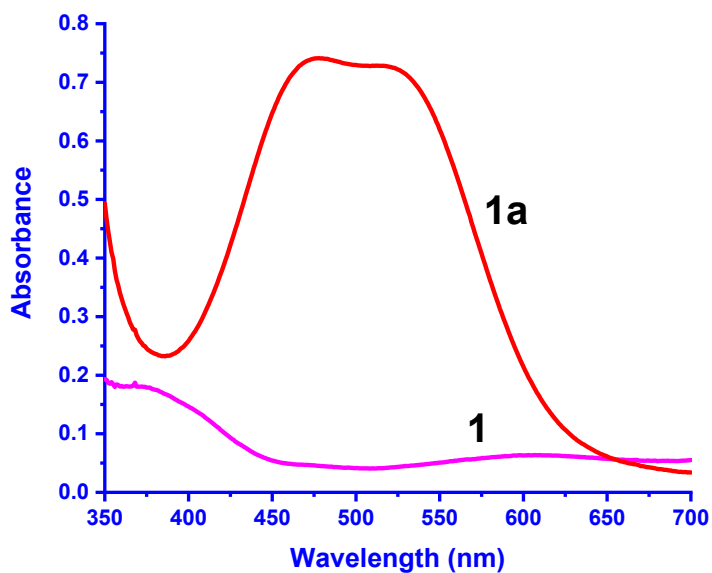


Fig. S11. Electronic absorption spectra of complexes **1** and the intermediate **1a** formed from **1** in methanol solution upon addition of Et_3N (2×10^{-4} M) to **1** (1×10^{-4} M) at 25 °C.

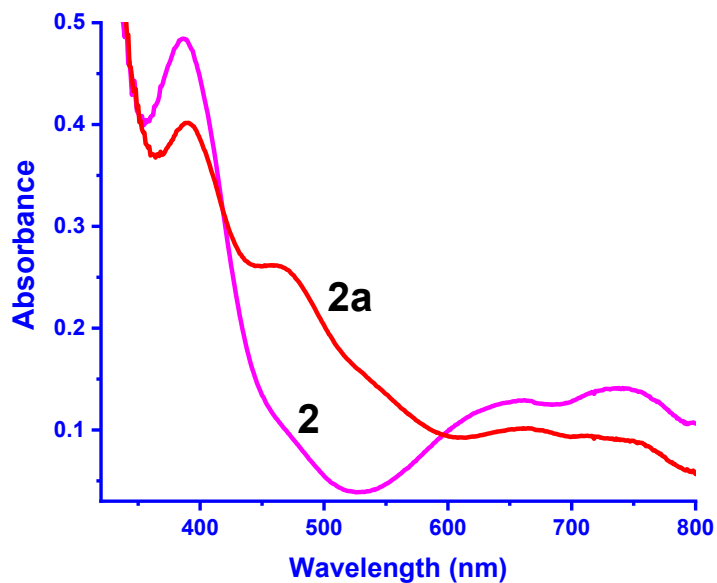


Fig. S12. Electronic absorption spectra of **2** and the intermediate **2a** formed from **2** in methanol solution upon addition of Et_3N (2×10^{-4} M) to **2** (1×10^{-4} M) at 25 °C.

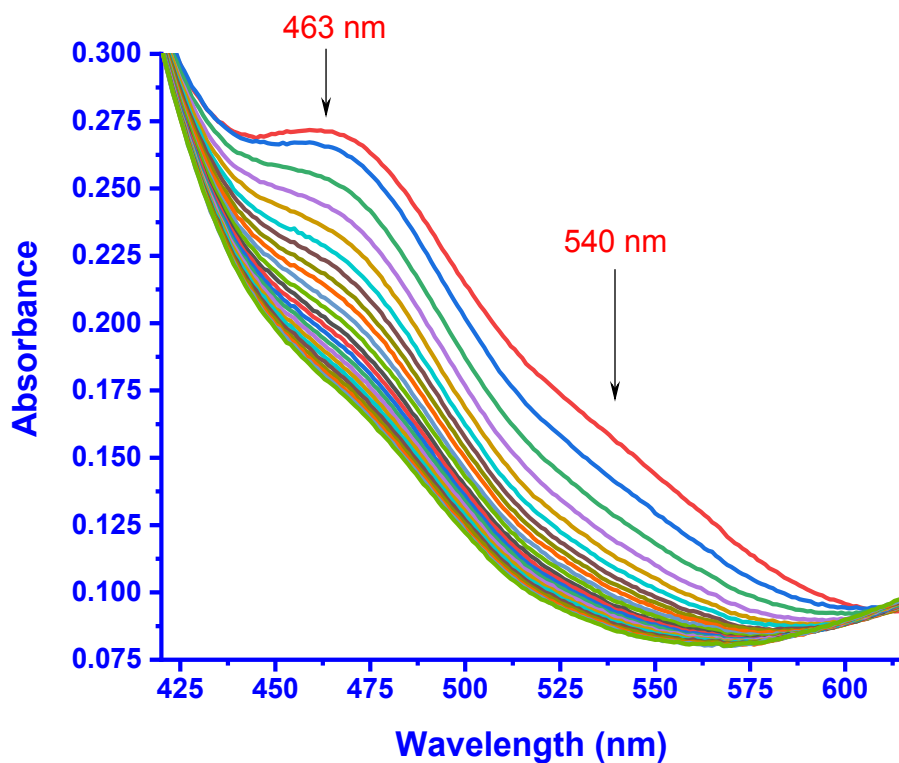


Fig. S13. Decrease in absorption of **2a**, generated in situ by adding Et_3N (4×10^{-4} M) to **2** (2×10^{-4} M), upon exposure to atmospheric CO_2 , followed at 1 min interval at 25°C .

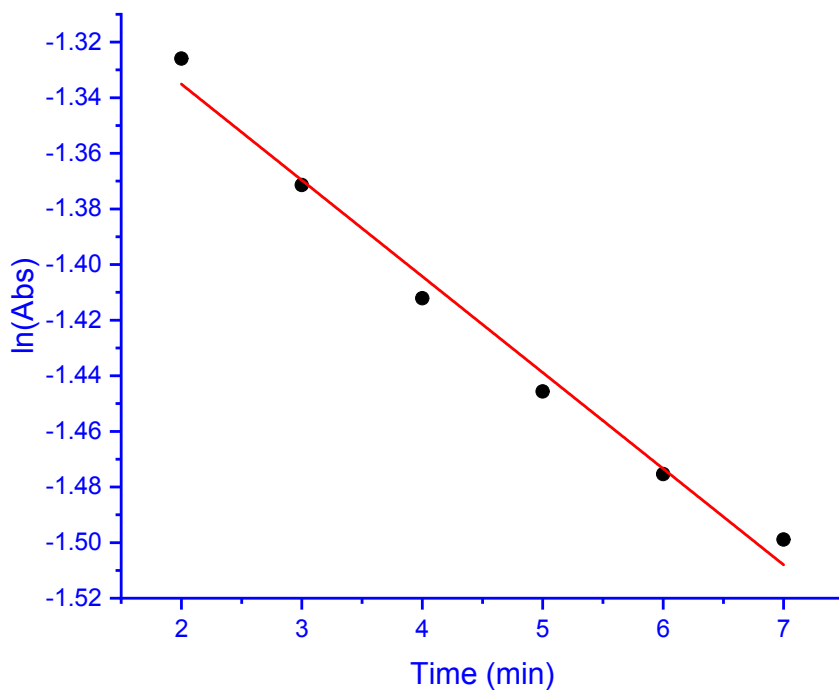


Fig. S14. Plot of $\ln(\text{Abs})$ vs time observed at 463 nm, k_{obs} , $5.8 \pm 0.3 \times 10^{-4} \text{ s}^{-1}$; $t_{1/2} = 0.33$ hrs.

Table S3. Computed structural parameters of the HOMO and LUMO energy values for the intermediate complex species **1a** and **2a**

	1a	2a
HOMO-2 (eV)	-7.2507	-6.9416
HOMO-1 (eV)	-6.6023	-6.5294
HOMO (eV)	-6.3604	-6.2700
LUMO (eV)	-1.8444	-1.6393
LUMO+1 (eV)	-1.6501	-0.4705
LUMO+2 (eV)	-1.2139	-0.1295

Table S4. Computed energy gap values for complexes **1a** and the intermediate **2a**

Band gap (eV)	1a	2a
HOMO – LUMO (eV)	4.5160	4.6307
LUMO – LUMO+1 (eV)	0.1943	1.1688

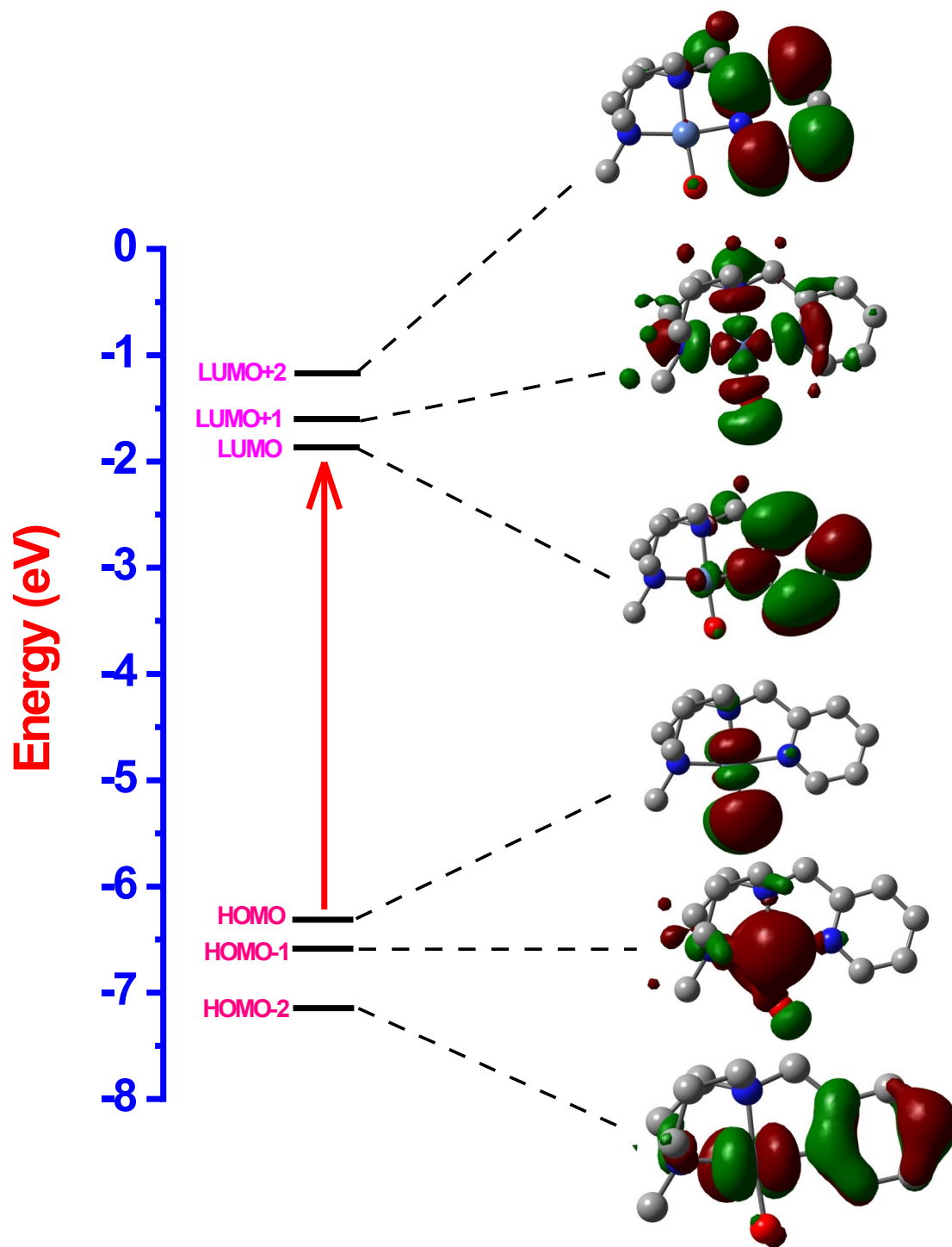


Fig. S15. Schematic MO diagram for the intermediate complex 1a

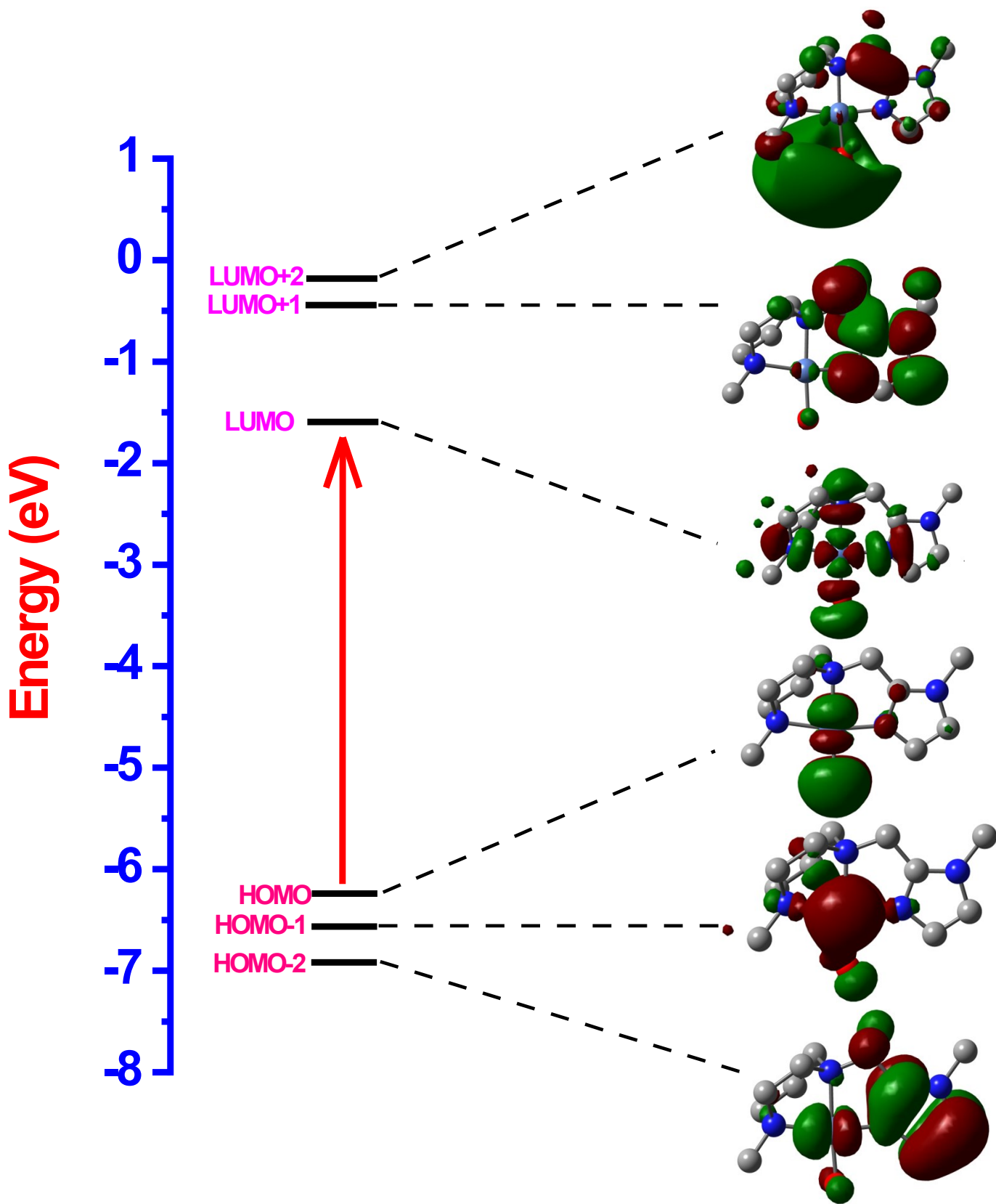
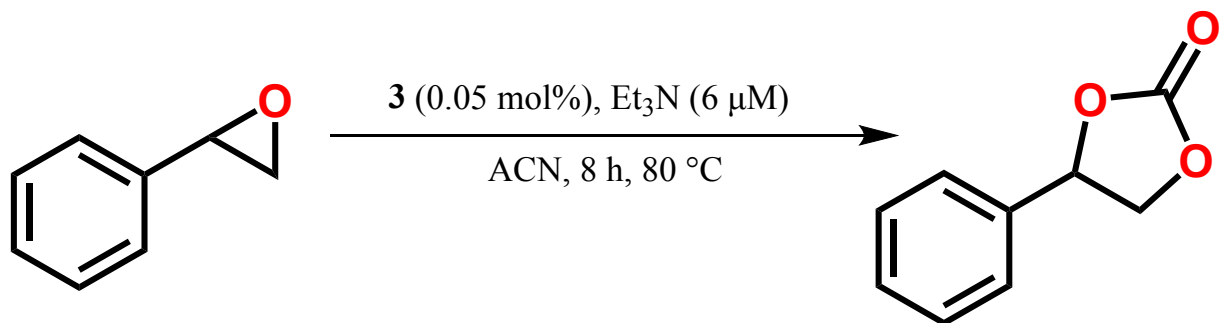


Fig. S16. Schematic MO diagram for the intermediate complex species 2a



Scheme S1. Conversion of epoxide into cyclic carbonates.

Table S5. Reaction of Styrene epoxide (10 mmol) with 1 atm pure CO₂ using catalyst **3** (0.05 mol%) and Et₃N as a base (6 μM) for a period of 8 hrs.

Entry	Temperature (°C)	Yield (%)	TON	TOF (h ⁻¹)	Selectivity (%)
1	30	9	180	23	>99
2	40	25	500	63	>99
3	50	39	780	98	>99
4	60	55	1100	138	>99
5	80	72	1440	180	>99

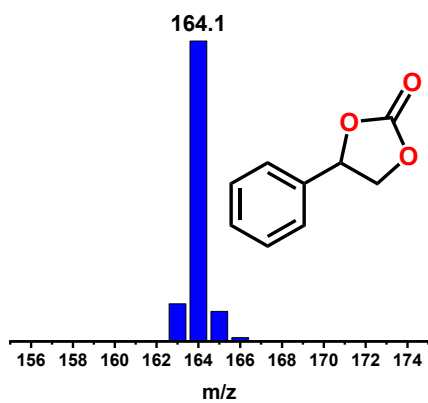


Fig. S17. GC-MS spectra of 4-phenyl-1,3-dioxolan-2-one.

42 #32 RT: 0.31 AV: 1 NL: 6.27E9

T: FTMS + p ESI Full ms [133.4000-2000.0000]

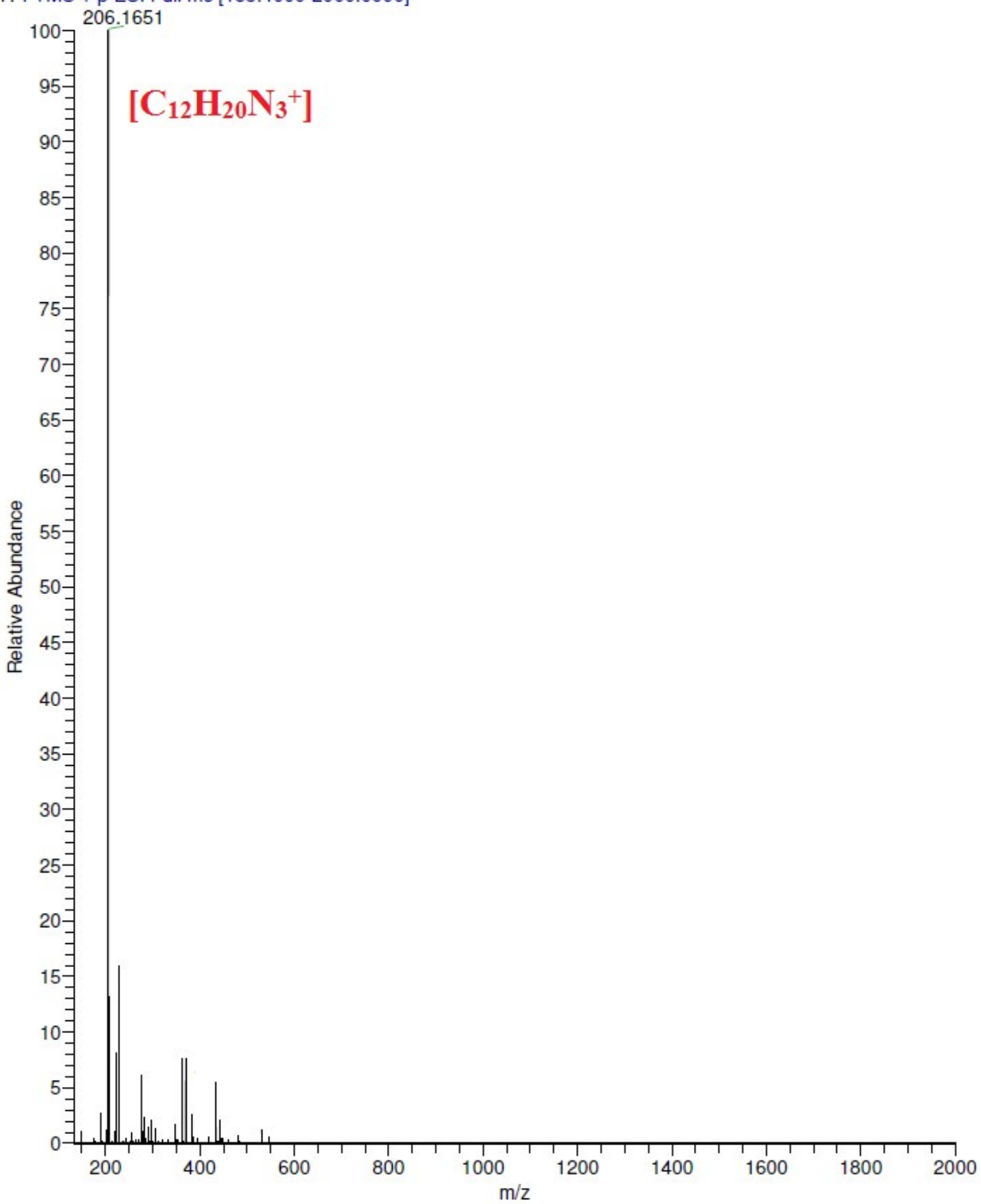


Fig. S18. High Resolution Mass Spectra of L1 in methanol solution (1×10^{-3} M) at 25 °C.

Hm-Im-3N #47 RT: 0.46 AV: 1 NL: 9.35E9
T: FTMS + p ESI Full ms [100.0000-1500.0000]

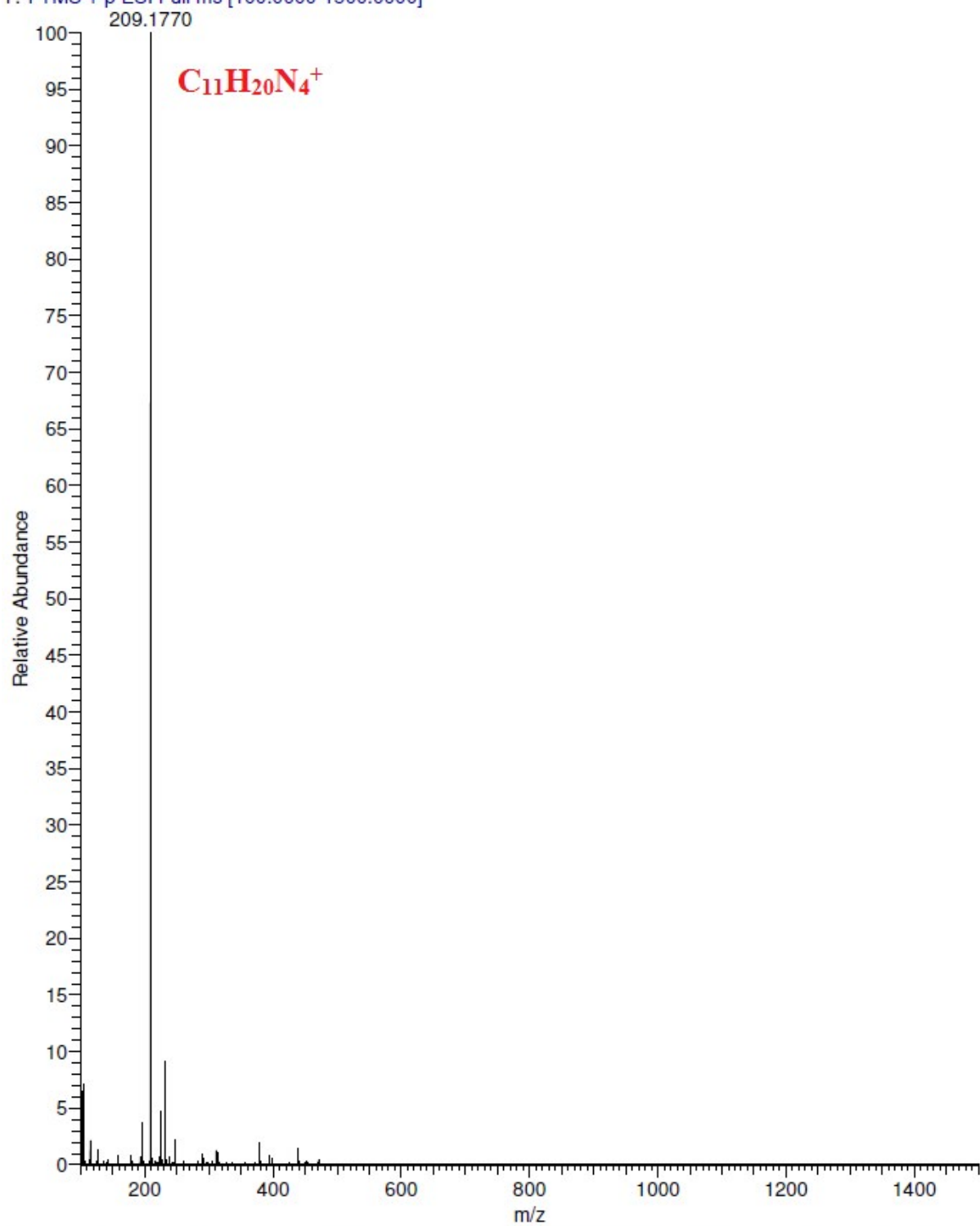


Fig. S19. High Resolution Mass Spectra of L2 in methanol solution (1×10^{-3} M) at 25 °C.

Ni-Hm-Py-3N #35 RT: 0.35 AV: 1 NL: 3.46E9
T: FTMS + p ESI Full ms [100.0000-1500.0000]

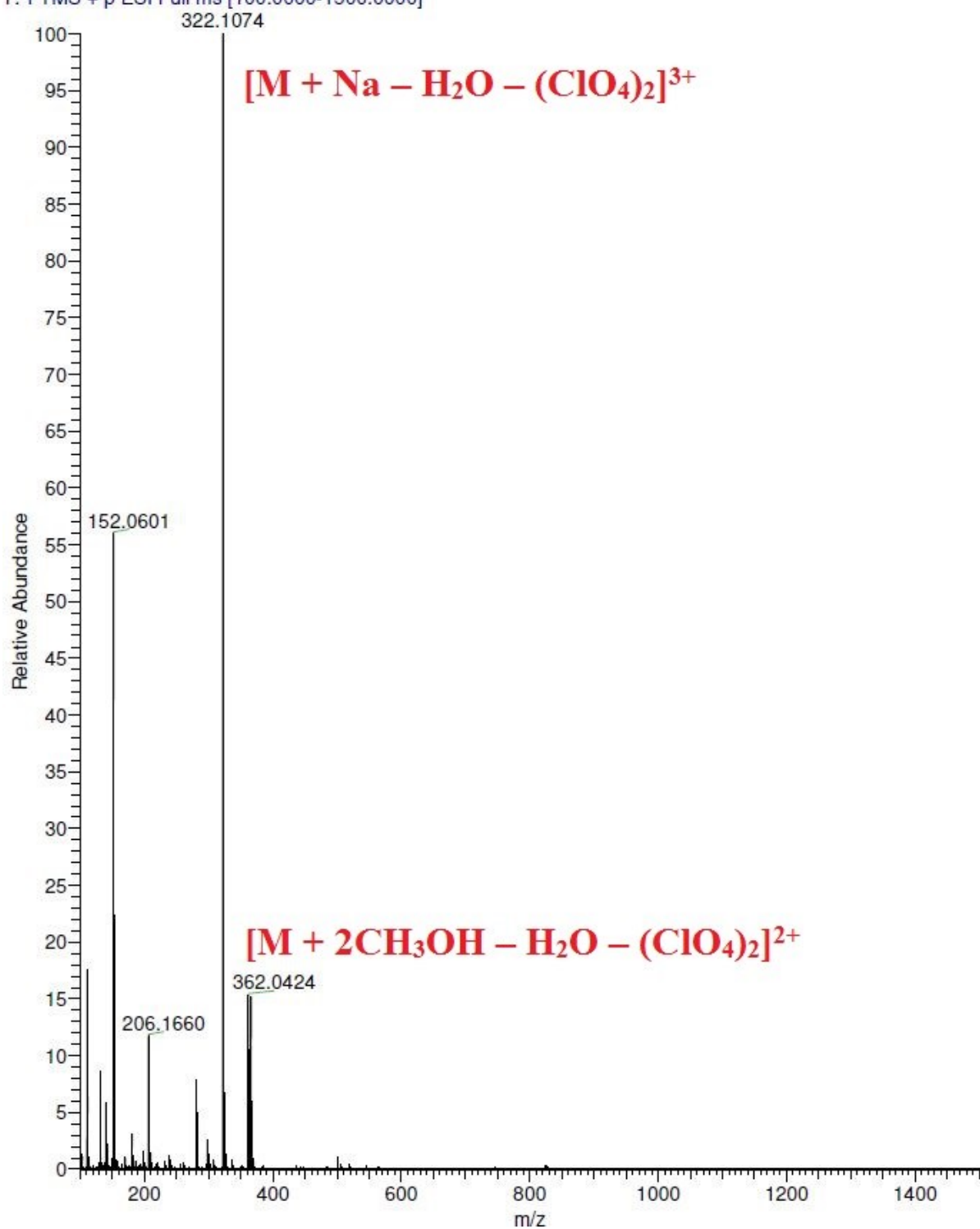


Fig S20. High Resolution Mass Spectra of $[Ni(L1)(H_2O)_3](ClO_4)_2$ **1** in methanol solution (1×10^{-3} M) at 25 °C.

Ni-HM-In-3N #33 RT: 0.33 AV: 1 NL: 1.02E9
T: FTMS - p ESI Full ms [150.0000-2000.0000]

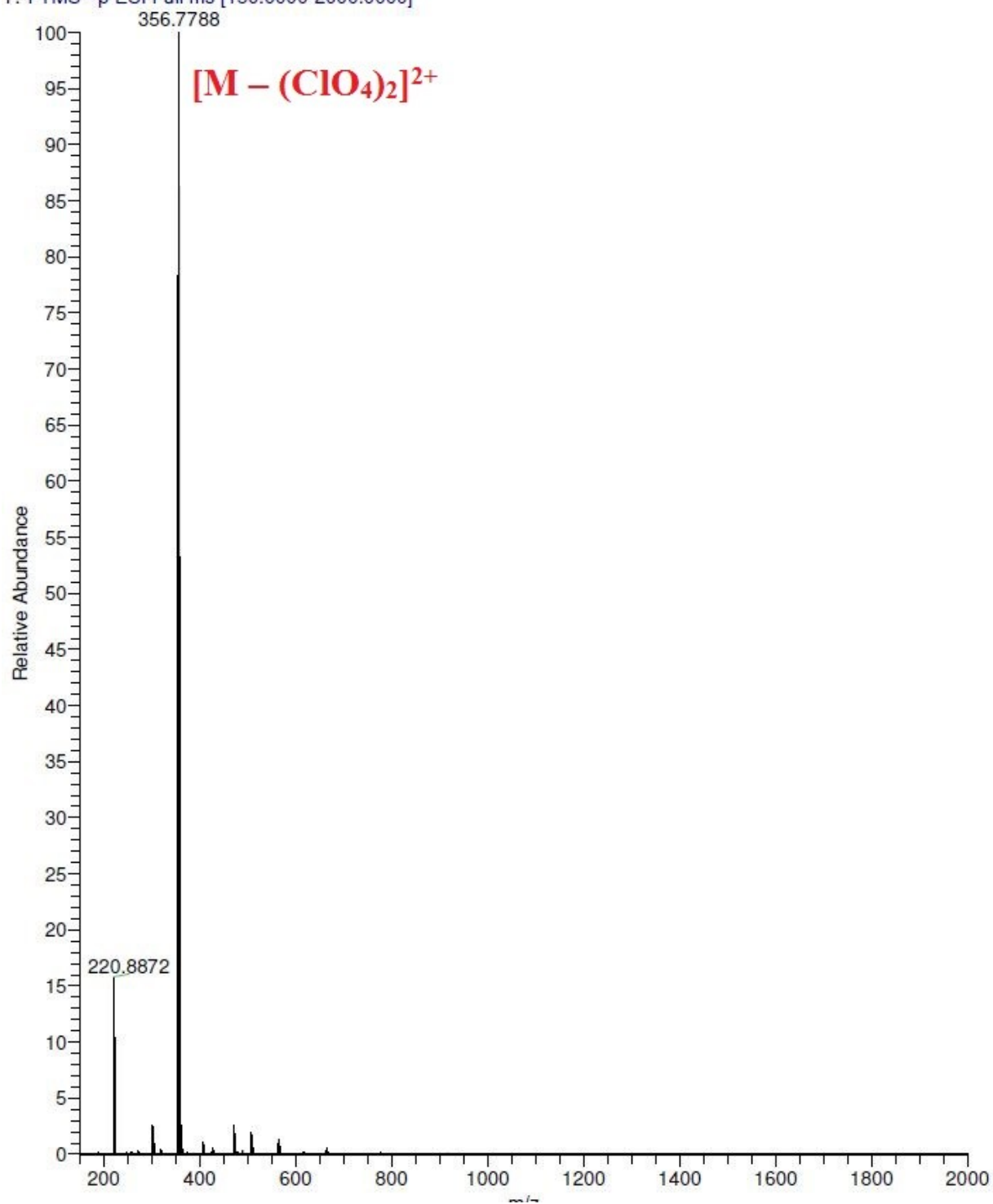


Fig. S21. High Resolution Mass Spectra $[Ni(L2)(H_2O)_3](ClO_4)_2 \cdot 2H_2O$ **2** in methanol solution (1×10^{-3} M) at 25 °C.

Di-Ni-MeOH #37 RT: 0.37 AV: 1 NL: 2.26E9
T: FTMS + p ESI Full ms [100.0000-1000.0000]

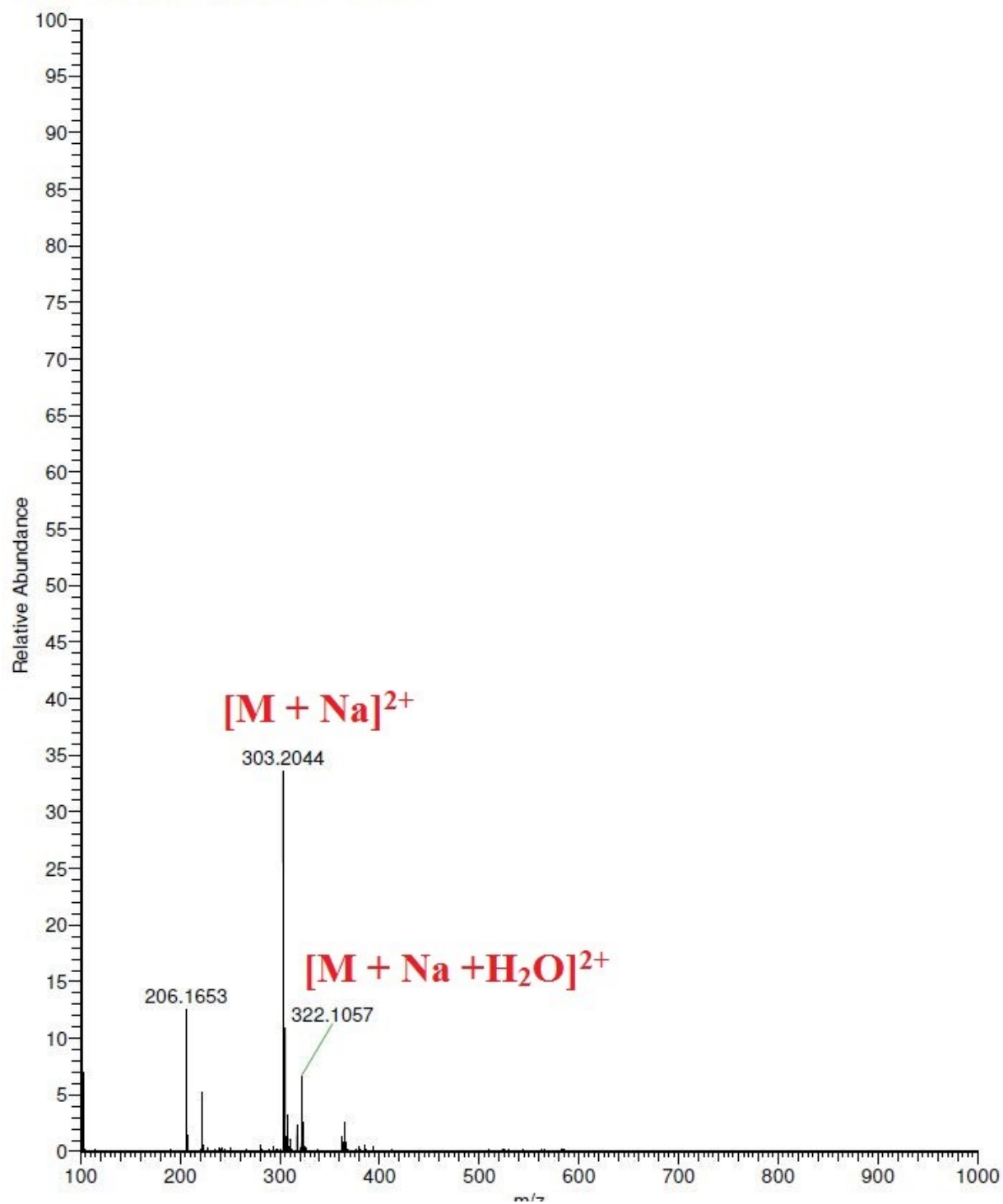


Fig. S22. High Resolution Mass Spectra of intermediate **1a** methanol solution (1×10^{-3} M) at 25 °C.

Di-Ni-EtOH #37 RT: 0.36 AV: 1 NL: 1.80E9
T: FTMS + p ESI Full ms [100.0000-1000.0000]

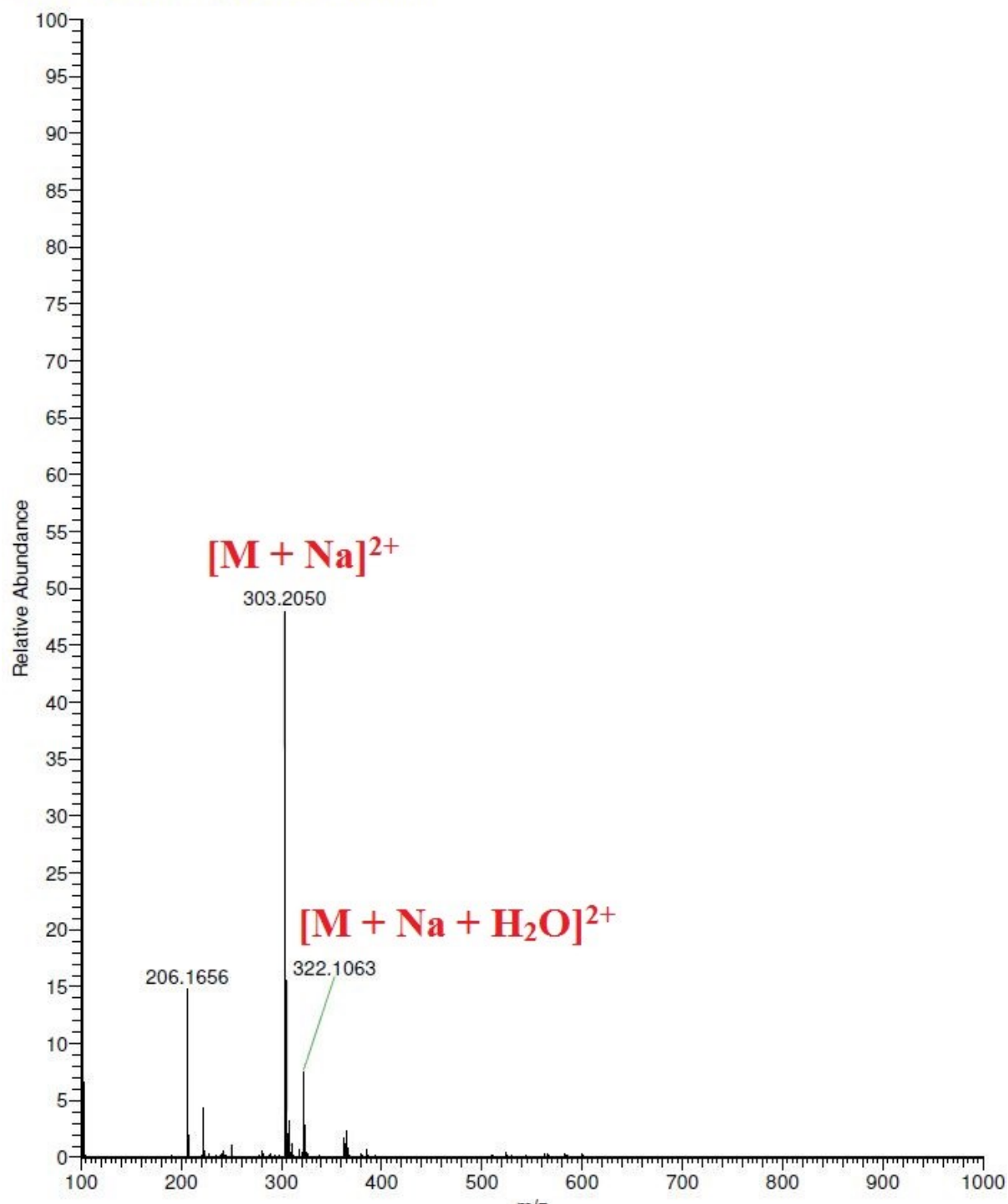


Fig. S23. High Resolution Mass Spectra of the intermediate **1a** in ethanol solution (1×10^{-3} M) at 25 °C.

Ni-Py #37 RT: 0.36 AV: 1 NL: 2.32E9
T: FTMS + p ESI Full ms [100.0000-1000.0000]

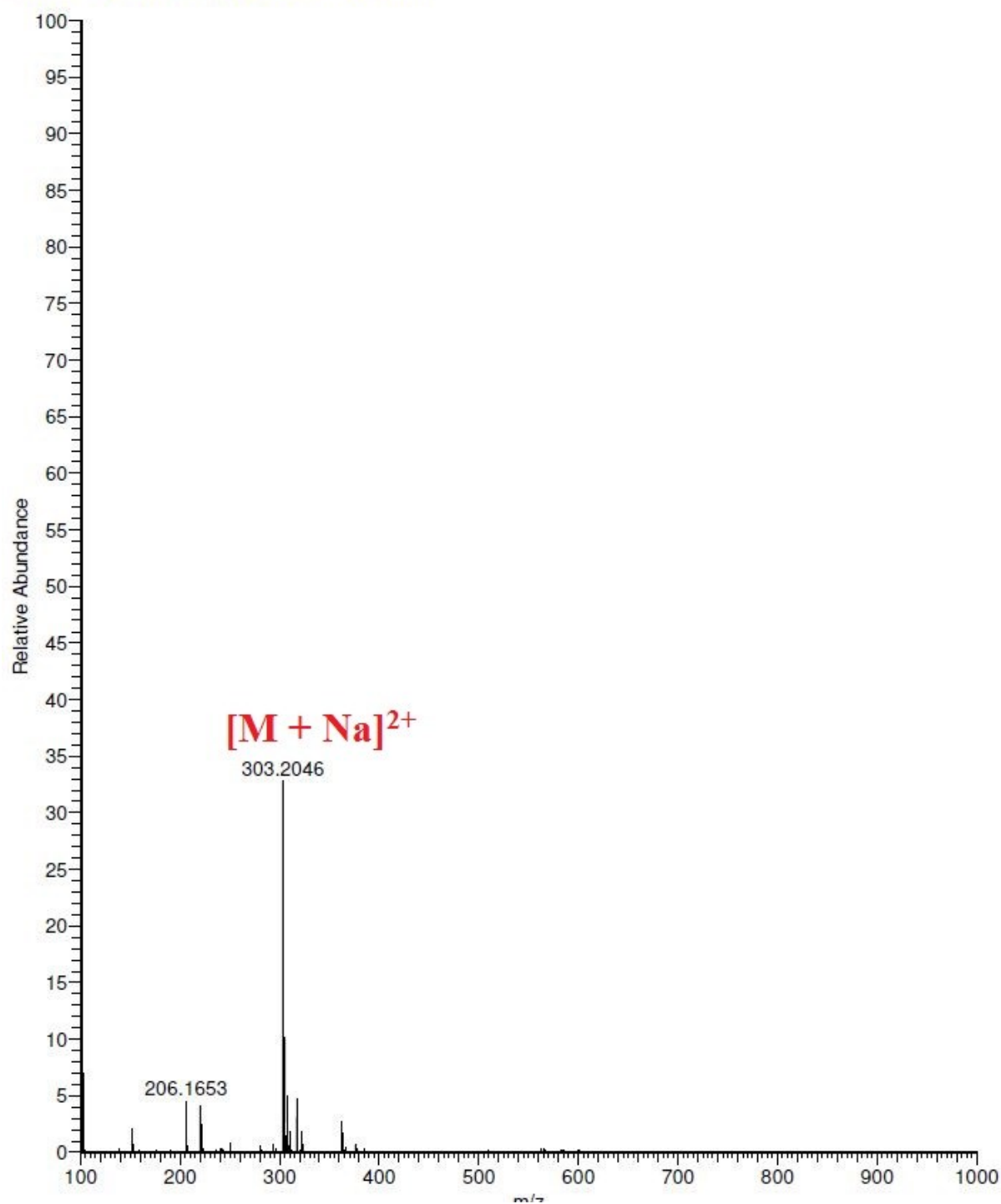


Fig. S24. High Resolution Mass Spectra of the intermediate **1a** in isopropanol solution (1×10^{-3} M) at 25 °C.

dini-Hmpy #44 RT: 0.43 AV: 1 NL: 2.02E9
T: FTMS + p ESI Full ms [150.0000-2000.0000]

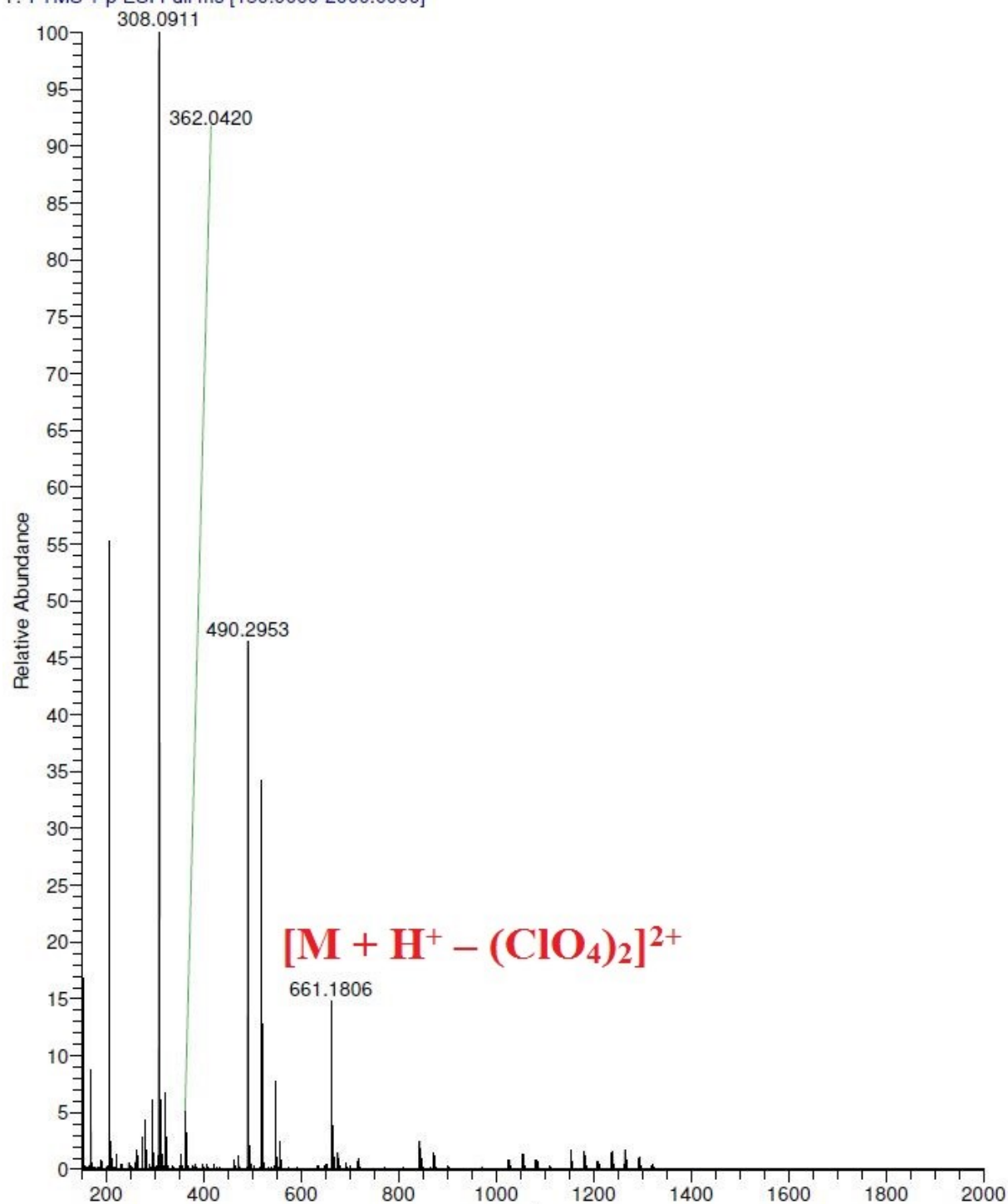


Fig. S25. High Resolution Mass Spectra of $[Ni_2(L1)_2(\mu-CO_3)(H_2O)_2](ClO_4) \cdot 2H_2O$ **3** in methanol solution (1×10^{-3} M) and at 25 °C.

References

S1. D. F. Evans, *J. Chem. Soc.* 1959, 2003-2005.

S2. J. Lölinger, R. Scheffold, *J. Chem. Edu.*, 1972, 646-647.